COMMUNICATION

Chinese Journal of Structural Chemistry

Strong High Entropy Alloy-Support Interaction Enables Efficient Electrocatalytic Water Splitting at High Current Density

Hongdong Li[1], Yue Pan[1], Jianping Lai[1]*, Lei Wang[1,2]* and Shouhua Feng[1]

[1]*Key Laboratory of Eco-chemical Engineering, Taishan Scholar Advantage and Characteristic Discipline Team of Eco-chemical Process and Technology, College of Chemistry and Molecular Engineering, Qingdao University of Science and Technology, Qingdao 266042, China*
[2]*Shandong Engineering Research Center for Marine Environment Corrosion and Safety Protection, College of Environment and Safety Engineering, Qingdao University of Science and Technology, Qingdao 266042, China*

ABSTRACT In electrocatalysis, the stability issue between catalyst and support still needs great attention. Here, a series of high-entropy alloy nanoparticles (HEA-NPs) embedded in carbon cloth (CC) were synthesized by using the scalable strategy-microwave heating. Among them, PtRhCoNiCu/CC exhibits outstanding hydrogen evolution reaction (HER) activity (19 and 170 mV overpotential at 10 and 1000 mA cm^{-2}) and stability (150 h), outperforming other recently reported HEAs catalysts. IrRuCoNiCu/CC displays superior oxygen evolution reaction (OER) activity (166 and 354 mV overpotential at 10 and 1000 mA cm^{-2}) and stability (150 h), and shows a lower overpotential than recently reported HEA catalysts. In water splitting, IrRuCoNiCu/CC(+)//PtRhCoNiCu/CC(-) electrolyzer achieves 500 mA cm^{-2} (1000 mA cm^{-2}) high current density at 1.76 V (1.88 V) and exhibits excellent stability, which is one of the best catalysts currently. Therefore, the novel supported HEA catalyst with high stability is expected to be a promising candidate material for industrialized water splitting.

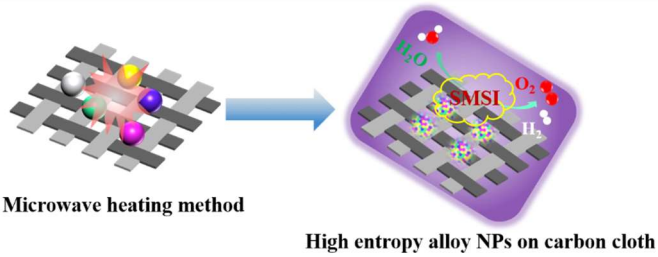

Keywords: high entropy alloy, metal-support interactions, microwave heating, water splitting, activity and durability

INTRODUNTION

High-entropy alloys (HEAs) have attracted extensive attention in the fields of energy and catalysis due to their unique "cocktail" effect and abundant active sites.[1-8] Although HEAs nanoparticles (NPs) exhibit excellent anti-dissolution properties and good stability due to the entropy stabilization effect,[7,9,10], in practical applications, the problem of HEA-NPs agglomeration is also an urgent concern.[9,11] In the field of electrocatalysis, carbon materials are usually selected as supports because of their large specific surface area, high electrical conductivity and low cost.[12-15] HEA-NPs are usually supported on carbon supports by physical mixing, though the problem of particle agglomeration can be improved to some extent. However, the interaction between NPs and the carbon support is weak.[9,16-18] After long-term operation, the HEA-NPs will also agglomerate, causing the loss of active sites and the degradation of catalytic performance. To solve this problem, much more efforts have been devoted to enhancing the stability of supports and HEA-NPs. For example, Hu et al. synthesized stable multi-elemental alloy NPs on carbon support by introducing metal oxides.[9] However, the introduction of oxides may reduce the electrical conductivity of the material and affect its catalytic performance in electrocatalysis, also increasing the catalyst cost. Therefore, it is crucial to develop new strategies to prepare efficient and stable carbon-supported HEA catalysts.

According to reports, strong metal-support interaction (SMSI) exhibits the characteristics of the support components covering or encapsulating metal NPs, which can effectively inhibit the aggregation and shedding of nanoparticles, thereby improving the stability of catalysts.[19-26] Therefore, it can be used as an effective strategy to prepare highly stable supported catalysts. The HEA-NPs can be confined in carbon support: i) the conductive carbon support can enhance the charge transfer ability,[27,28] ii) the strong interaction between the active components (HEA-NPs) and the carbon support can enhance its stability.[29] However, the traditional synthesis method of HEAs requires a long time or cumbersome operation, and it is difficult to control the metal-support interface. Therefore, to improve the performance of supported catalysts and make them suitable for practical applications, it is necessary to develop an economical, efficient, and large-scale preparation method.

Microwave heating as an internal heat source has been widely used in the rapid preparation of many nanomaterials (carbon materials and carbon supported nanomaterials).[22,30-33] This method has a series of advantages, such as high temperature, fast heating and cooling speed, uniform heating distribution, suitability for various sizes of carbon materials and economic.[30,34] Herein, we develop a general method for the rapid synthesis of stable HEA-NPs on carbon supports (carbon cloth, CC) by rapid microwave heating. The HEA-NPs were directly grown and firmly confined on the CC, and the NPs were well dispersed. To evaluate the performance of designed catalysts, water splitting performance tests were carried out. Among them, PtRhCoNiCu/CC shows excellent HER performance, with a low overpotential of 170 mV at 1000 mA cm^{-2} and a TOF value of 0.49 s^{-1} at the 100 mV overpotential. In addition, IrRuCoNiCu/CC exhibits outstanding OER performance (354 mV overpotential at 1000 mA cm^{-2}, and the TOF value reaches 0.28 s^{-1} at 300 mV

DOI: 10.14102/j.cnki.0254-5861.2022-0125

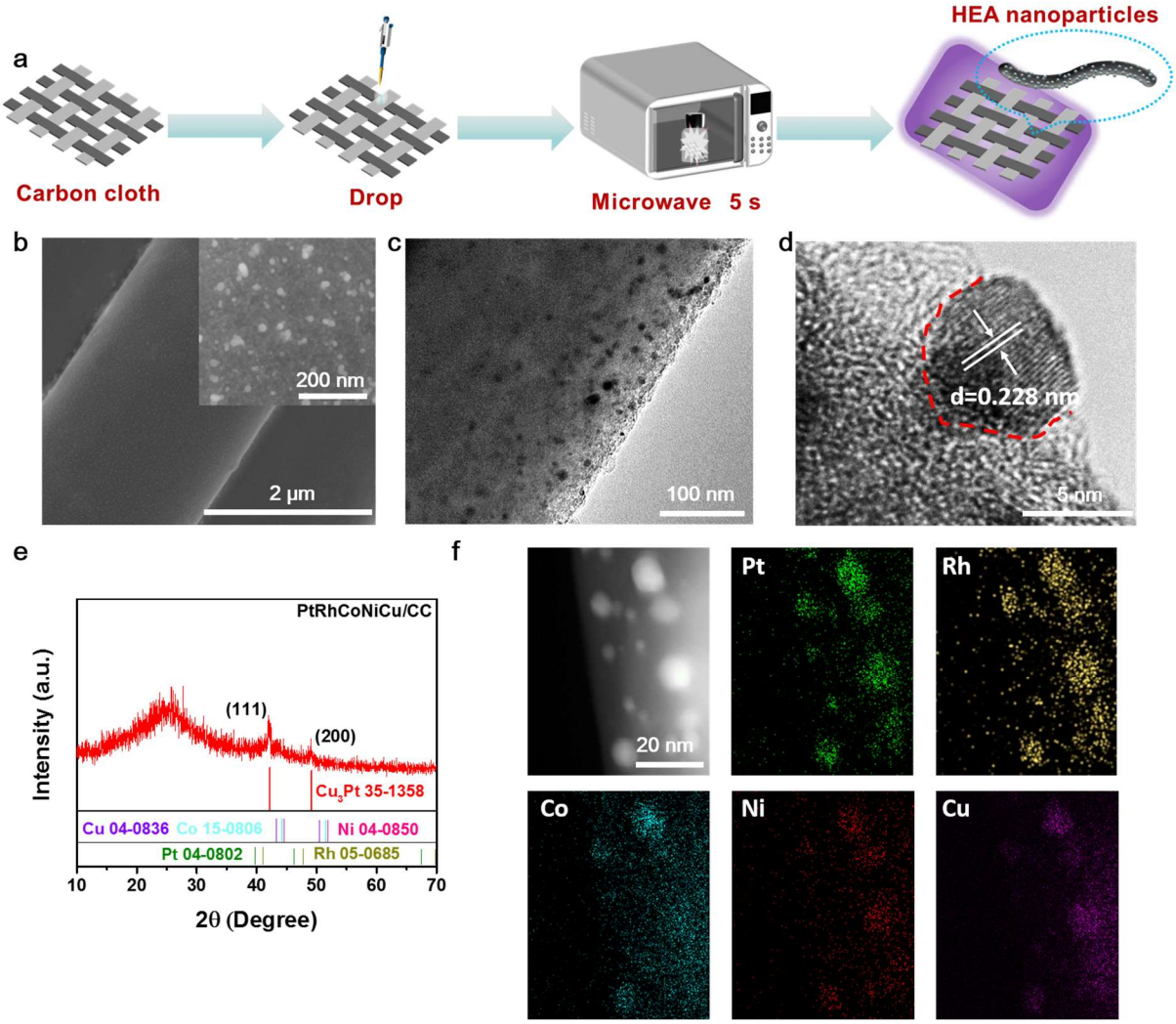

Figure 1. (a) Schematic for the synthesis of HEA-NPs/CC. (b) SEM images, (c) TEM image, (d) HRTEM image, (e) XRD and (f) Elemental mapping of PtRhCoNiCu/CC.

overpotential). Importantly, HEAs-NPs/CC catalysts also demonstrate excellent stability at high current density. In water splitting, IrRuCoNiCu/CC//PtRhCoNiCu/CC has high current density up to 1000 mA cm^{-2} at 1.88 V and diaplays excellent stability of 100 h, superior to RuO_2/CC//Pt/C/CC.

RESULTS AND DISCUSSION

A series of HEA-NPs partially embedded in CC were prepared by a facile, fast microwave method. As shown in the schematic of the synthesis process (Figure 1a), the metal salt mixed solution was dropped directly onto the CC and the precursor/CC was sealed in a glass bottle for microwave heating (Figure S1). Importantly, after a few seconds (about 10 s), the NPs material embedded in CC can be obtained. As we know, Pt, Ru, and Rh-based catalysts showed excellent HER activity.[35-41] Ir- and Ru-based catalysts displayed outstanding OER activity.[42-45] On the other hand, transition metal-based (Fe, Co, Ni, Cu, et al.) catalysts (metal oxides and hydroxides) also showed certain HER and OER activities.[39,46-53] Transition metals are also abundant on earth and easily mix with precious metals to form alloys.[54-56] Therefore, we prepared a series of HEA-NPs partially embedded in CC as catalysts for HER and OER.

As shown in Figure S2, the surface of CC appears partial depression after microwave treatment, which may anchor metal NPs to prevent their aggregation and improve their dispersity. From Figure 1b and c, the PtRhCoNiCu NPs are evenly distributed on CC, and the size of NPs is about 9.4 nm (Figure S3). High-resolution transmission electron microscopy (HRTEM) image shows that HEA-NPs are face-centered cubic (FCC) phase, and the spacing of (111) lattice fringes is 0.228 nm (Figure 1d). From Figure 1b and d, it can be clearly seen that the HEA-NPs are half-encapsulated in the carbon layer, which is consistent with the classic SMSI effect characteristics (Metal nanoparticles are encapsulated by the carrier to prevent migration).[22,57,58] It is preliminarily believed that SMSI may be generated between HEA and carbon carrier. In X-ray diffraction (XRD) patterns (Figure 1e), the two obvious diffraction peaks correspond to the (111) and (200) facets of fcc structure. Com-

DOI: 10.14102/j.cnki.0254-5861.2022-0125

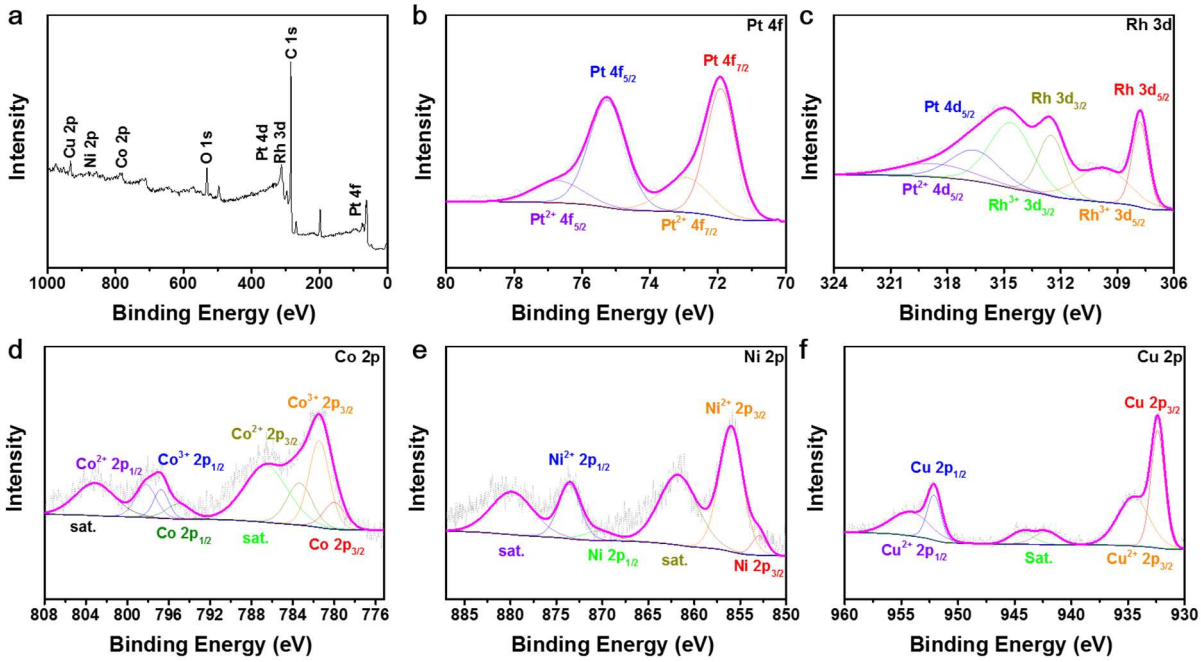

Figure 2. XPS compositional analysis of PtRhCoNiCu/CC sample. (a) XPS survey spectrum. (b) Pt 4f XPS spectrum. (c) Rh 3d XPS spectrum. (d) Co 2p XPS spectrum. (e) Ni 2p XPS spectrum. (f) Cu 2p XPS spectrum.

pared with the diffraction peaks of pure Pt, Rh, Co, Ni and Cu, the positions of diffraction peaks of PtRhCoNiCu/CC are shifted, which are consistent with those of Cu_3Pt alloy, indicating the synthesis of single-phase alloy (HEA). The TEM energy-dispersive X-ray spectroscopy (TEM-EDX) elemental maps of the PtRhCoNiCu NPs show that Pt, Rh, Co, Ni, and Cu are uniformly distributed across the NPs (Figure 1f), with the elemental ratio in PtRhCoNiCu/CC to be 32:22:11:15:20 (Table S1). The surface element states of HEA-NPs were analyzed by X-ray electron spectroscopy (XPS). By taking PtRhCoNiCu HEA-NPs sample as an example (Figure 2), Pt and Rh mainly exist in metallic state due to their high stability (Figure 2b-c). The Ni and Co on the surface of NPs mainly exist in the form of oxidation state, with a small amount of metal state (Figure 2d-e). The metallic Pt appears at 71.9 eV (Pt $4f_{7/2}$) and 75.2 eV (Pt $4f_{5/2}$) (Figure 2b). Compared with Pt/CC, the peak of Pt^0 in the PtRhCoNiCu/CC sample showed a negative shift (Figure S4), indicating the electron transfer between Pt and other metals. The peaks present at 312.5 eV (Rh $3d_{3/2}$) and 307.8 eV (Rh $3d_{5/2}$) can be ascribed to metallic Rh, and those at 314.6 eV (Rh $3d_{3/2}$) and 309.8 eV (Rh $3d_{5/2}$) belong to Rh^{3+} state (Figure 2c).[59] The Co 2p peaks have three valence states of Co^0 (779.8 eV, Co $2p_{3/2}$), Co^{2+} (783.3 eV, Co^{2+} $2p_{3/2}$) and Co^{3+} (781.4 eV, Co^{3+} $2p_{3/2}$) (Figure 2d). The Ni 2P spectra showed that it is mainly in the form of Ni^{2+} (855.9 eV, Ni^{2+} $2p_{3/2}$) with a small amount of Ni^0 (852.7 eV, Ni $2p_{3/2}$). The Cu 2p spectra also exhibit Cu^0 (932.3 eV, Cu $2p_{3/2}$) and Cu^{2+} (934.4 eV, Cu^{2+} $2p_{3/2}$) peaks coexisting in the sample (Figure 2f).

To further prove the universality of microwave heating method, we synthesized a series of HEA (PtRuCoNiCu, PtIrCoNiCu, PtFeCoNiCu, IrRuCoNiCu, IrRhCoNiCu, RuRhCoNiCu, RuFeCoNiCu, RhFeCoNiCu, and IrFeCoNiCu) NPs on CC (Figure S5-S7), which are uniformly distributed on CC. The elemental ratio in HEA-NPs is shown in Table S1. In addition, we also characterize the IrRuCoNiCu HEA-NPs to verify the successful preparation of the designed materials. From SEM and TEM images as well as XRD and EDX elemental maps (Figure S8), IrRuCoNiCu NPs with FCC structure are uniformly distributed on CC, and Ir, Ru, Co, Ni, and Cu elements are evenly distributed. Importantly, the NPs are also semi-encapsulated in the carbon layer (Figure S8a and d). Further, the as-prepared HEA-NPs on CC were studied as bifunctional electrocatalysts for HER and OER in alkaline solutions, and the optimal catalysts were selected for overall water splitting.

The HER performance of different samples in 1.0 M KOH solution was investigated. As expected, HER activity of HEA-NPs/CC catalysts is significantly increased. For comparison, Pt/C catalyst was fixed on CC (Pt/C/CC) to test HER polarization curve. Figure 3a and Figure S9a show the HER polarization linear sweep voltammetry (LSV) curves of HEA-NPs/CC and Pt/C/CC. Among them, PtRhCoNiCu/CC catalyst exhibits superior HER activity, only taking low overpotentials of 19 and 170 mV at 10 and 1000 mA cm^{-2}, which is better than the commercial Pt/C (η_{10} = 30 mV, η_{1000} = 315 mV). In addition, at 1000 mA cm^{-2}, the overpotentials of RuRhCoNiCu/CC, RhFeCoNiCu/CC, IrRhCoNiCu/CC, PtRuCoNiCu/CC, RuFeCoNiCu/CC, IrRuCoNiCu/CC, PtIrCoNiCu/CC, and PtFeCoNiCu/CC and Pt/C/CC are 187, 208, 217, 219, 237, 244, 250, 297, and 314 mV, respectively (Figure 3b). Moreover, the mass activity of PtRhCoNiCu/CC was significantly increased (Figure 3c). At -0.05 V vs. RHE, the mass activity of PtRhCoNiCu/CC is 244.9 mA mg^{-1}_{matal}, higher than that of Pt/C/CC and other HEA-NPs/CC

Chin. J. Struct. Chem. **2022**, 41, 2208003-2208011
DOI: 10.14102/j.cnki.0254-5861.2022-0125

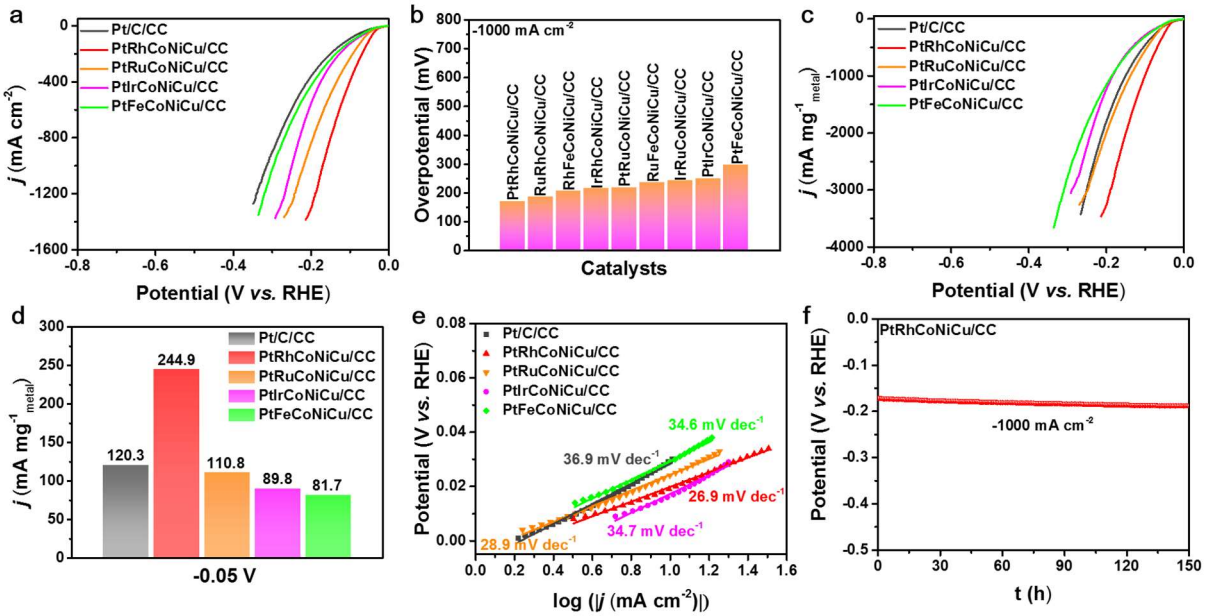

Figure 3. Electrocatalytic performance of HER in 1.0 M KOH. (a) LSV curves, (b) comparisons of HER overpotentials, (c) mass activity of LSV curves, (d) the mass activities at the potential of -0.05 V *vs.* RHE, and (e) Tafel curves for Pt/C/CC and HEA-NPs/CC. (f) CP curve of PtRhCoNiCu/CC at -1000 mA cm^{-2}.

(Figure 3d and Figure S9). Importantly, the HER performance of PtRhCoNiCu/CC is superior to that for other recently reported HEAs catalysts in alkaline media (Table S3). These results show that HEA-NPs/CC catalyst can meet the requirements of high current density catalytic activity in industrial scale.

The Tafel slope can be used to study the kinetics of HER. Small Tafel value indicates that the catalyst can overcome the HER kinetic process.[60] From Figure 3e and Figure S9b, we can see that the Tafel slope of PtRhCoNiCu/CC is 26.9 mV dev^{-1}, which is smaller than that of PtRuCoNiCu/CC (28.9 mV dev^{-1}), PtIrCoNiCu/CC (34.7 mV dev^{-1}), RuRhCoNiCu/CC (27.2 mV dev^{-1}), IrRhCoNiCu/CC (28.4 mV dev^{-1}), IrRuCoNiCu/CC (30.4 mV dev^{-1}), PtFeCoNiCu/CC (34.6 mV dev^{-1}), RuFeCoNiCu (32.0 mV dev^{-1}), RhFeCoNiCu (28.2 mV dev^{-1}), IrFeCoNiCu/CC (37.3 mV dev^{-1}) and Pt/C/CC (36.9 mV dev^{-1}). The Tafel slopes for HEA-NPs/CC are 26-40 mV dec^{-1}, respectively, suggesting the Tafel step is the rate-limiting step. As comparison, the Tafel slope of PtRhCoNiCu/CC reaches 26.9 mV dec^{-1}, revealing water dissociation kinetics has been substantially boosted. The double-layer capacitance (C_{dl}) obtained by the cyclic voltammetry (CV) method and the turnover frequency (TOF) can evaluate the intrinsic activity of the catalyst.[60] The HEA-NPs/CC catalysts show higher C_{dl} value than Pt/C/CC (Figure S10-S11), indicating that it can expose more active sites, effectively improve the intrinsic activity and accelerate the HER process. Among them, the PtRhCoNiCu/CC (31.3 mF cm^{-2}) catalyst has the largest C_{dl} value. In addition, the intrinsic activity of catalyst was evaluated by TOF. From Figure S12, the TOF value of PtRhCoNiCu/CC reaches 0.49 s^{-1} at 100 mV overpotential for HER, which is higher than that of other HEA-NPs/CC catalysts. Obviously, the intrinsic catalytic activity of PtRhCoNiCu/CC is superior to that of other catalysts for HER.

In order to study the stability of PtRhCoNiCu/CC catalyst, we performed the CP test continuously for 150 h at a current density of 1000 mA cm^{-2} (Figure 3f), and the potential did not change significantly, indicating superior stability of the catalyst. Figure S13 shows fluctuations in potential curve caused by generation and escape of huge amounts of bulbbles at high current densities. In addition, comparing the LSV before and after 10,000 cycles (Figure S14), the overpotential is negligibly changed at 1000 mA cm^{-2} (170 and 178 mV), demonstrating the extraordinary electrochemical stability. From the SEM (Figure S15a-b) and TEM images (Figure S15c), the morphology and sizes (Figure S15d) of PtRhCoNiCu/CC do not change significantly. In addition, the XPS spectra of PtRhCoNiCu/CC (Figure S16) reveal that its elements maintained almost identical chemical states as compared to the that before stability test. These results confirm that PtRhCoNiCu/CC catalyst exhibits excellent stability. The electrocatalytic activity and stability of HEA-NPs/CC catalyst were significantly improved, which may be attributed to chemical composition and structural characteristics.[2,61-64]

Importantly, the interaction between metal and support is often used to stabilize metal NPs in order to obtain high stability and long life.[65] The carbon cloth support confines the metal NPs and prevents their agglomeration through the catalysts with partial depressions formed during the microwave process. In order to verify the advantages of this structure, we drop PtRhCoNiCu NPs on the carbon cloth directly (PtRhCoNiCu-CC, Figure S17a), which has the same metal loading with PtRhCoNiCu/CC. From Figure S17b-f, PtRhCoNiCu-CC has similar acticity, Tafel slope and Cdl with PtRhCoNiCu/CC. However, PtRhCoNiCu/CC has higher stability than PtRhCoNiCu-CC, indicating that metal NPs embedded on CC ((interaction between metal and support) can effectively improve the stability of metal catalyst.

In addition, we also prepared the Pt/CC and PtRh/CC by same method (Figure S18). Compared with the Pt/CC and PtRh/CC

DOI: 10.14102/j.cnki.0254-5861.2022-0125

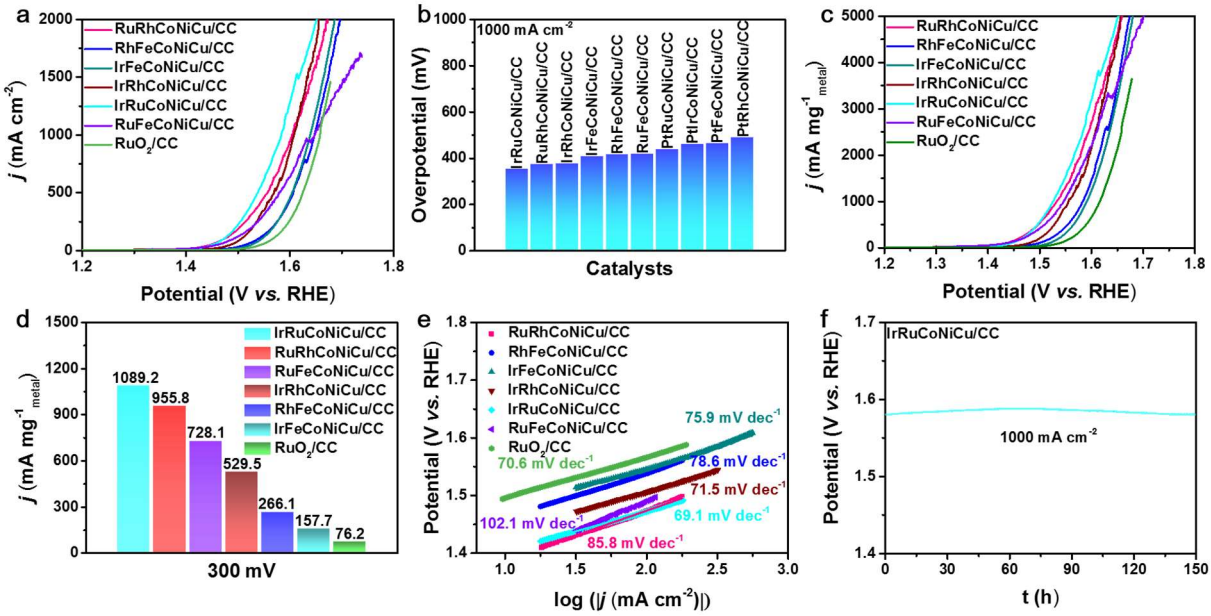

Figure 4. Electrocatalytic performance of OER in 1.0 M KOH. (a) LSV curves, (b) comparisons of OER overpotentials, (c) mass activity of LSV curves, (d) the mass activities at the 300 mV overpotential, and (e) Tafel curves for RuO_2/CC and HEA-NPs/CC. (f) CP curve of PtRhCoNiCu/CC at 1000 mA cm^{-2}.

catalysts, the HER activity of PtRhCoNiCu/CC was significantly improved (Figure S19a-c). The Tafel slope of PtRhCoNiCu/CC (26.9 mV dev^{-1}) is smaller than that of Pt/CC (31.4 mV dev^{-1}) and PtRh/CC (27.6 mV dev^{-1}) (Figure S19b). The results indicate that most HEA-NPs/CC catalysts can better overcome the HER kinetic process. Among them, the PtRhCoNiCu/CC (31.3 mF cm^{-2}) catalyst has the largest C_{dl} value (Figure S19d-f), and the enhanced activity of PtRhCoNiCu/CC may be attributed to the exposed more active sites.

From Figure S20 and Table S2, the Nyquist plots comprise one semicircle in the high frequency region, which is attributed to the charge-transfer resistance (Rct) resulting from the redox reaction on the electrocatalyst electrode. Rs is for the uncompensated solution resistance, which is about 5 Ω, indicating a similar electrolysis configuration. The PtRhCoNiCu/CC catalyst has a small semicircular diameter, indicating the small impedance and fast electron transport capability, which is beneficial to the improvement of HER performance.

The excellent HER performance of PtRhCoNiCu/CC catalyst can be attributed to chemical composition and structural characteristics. The existence of multi-active sites and synergistic effects in HEAs can facilitate electron transfer and intermediate transformation, and optimize the surface electronic structure and activity.[6,66,67] In PtRhCoNiCu/CC catalyst for HER, Pt and Rh are the main active sites of the catalyst, Ni and Co show good adsorption on H* and H_2O, and Cu could effectively promote the charge transfer within the catalyst.[41,53,64,68,69] In addition, the growth of nanomaterials on the supports is also important. CC support can also improve the accessibility of active sites of HEAs, further improve catalytic activity and contribute to high current density. In addition, directly preparing NPs on supports and confining them in CC can prevent their agglomeration, which can effectively improve the stability of catalysts.

Furthermore, we also evaluated the OER catalytic performance of the prepared catalysts in 1.0 M KOH solution. From Figure 4a-d and Figure S21, IrRuCoNiCu/CC catalyst displays the best performance, with only 166 and 354 mV overpotential at 10 and 1000 mA cm^{-2}. Its performance is better than that of other HEA-NPs/CC catalysts (IrRuCoNiCu/CC (η_{1000} = 354 mV) < RuRhCoNiCu/CC (η_{1000} = 374 mV) < IrRhCoNiCu/CC (η_{1000} = 378 mV) < IrFeCoNiCu/CC (η_{1000} = 409 mV) < RhFeCoNiCu/CC (η_{1000} = 417 mV) < RuFeCoNiCu/CC (η_{1000} = 418 mV) < PtRuCoNiCu/CC (η_{1000} = 438 mV) < PtIrCoNiCu/CC (η_{1000} = 460 mV) < PtFeCoNiCu/CC (η_{1000} = 465 mV) < PtRhCoNiCu/CC (η_{1000} = 490 mV)) and RuO_2/CC (η_{1000} = 428 mV). And the mass activity of IrRuCoNiCu/CC is up to 1089.2 mA mg^{-1}_{matal} at 300 mV overpotential, higher than that of other catalysts (Figure 4d and Figure S21d). Tafel slope was used to assess the dynamics of OER. Specifically, the Tafel slope is as follows: IrRuCoNiCu/CC (69.1 mV dev^{-1}) < RuO_2/CC (70.6 mV dev^{-1}) < IrRhCoNiCu/CC (71.5 mV dev^{-1}) < IrFeCoNiCu/CC (75.9 mV dev^{-1}) < RhFeCoNiCu/CC (78.6 mV dev^{-1}) < RuRhCoNiCu/CC (85.8 mV dev^{-1}) < PtFeCoNiCu/CC (88.9 mV dev^{-1}) < PtIrCoNiCu/CC (98.9 mV dev^{-1}) < RuFeCoNiCu/CC (102.1 mV dev^{-1}) < PtRuCoNiCu/CC (107.2 mV dev^{-1}) < PtRhCoNiCu/CC (125.9 mV dev^{-1}) (Figure 4e and Figure S21b). Due to the multicomponent properties, which reduced the amount of precious metals and increased activity, the IrRuCoNiCu/CC catalyst shows a lower overpotential than recently reported HEAs catalysts (Table S4). The Tafel slope of IrRuCoNiCu/CC catalyst is 69.1 mV dec^{-1}, which is also lower than the Tafel value of RuO_2 (70.6 mV dev^{-1}), indicating the best OER kinetics. From the value of Cdl (Figure S10-S11) and TOF (Figure S22), the IrRuCoNiCu/CC (32.0 mF cm^{-2}) catalyst has the largest C_{dl} value, and the TOF value reaches 0.28 s^{-1} at 300 mV overpotential. These results indicate that the IrRuCoNiCu/CC catalyst has high intrinsic activity, which

DOI: 10.14102/j.cnki.0254-5861.2022-0125

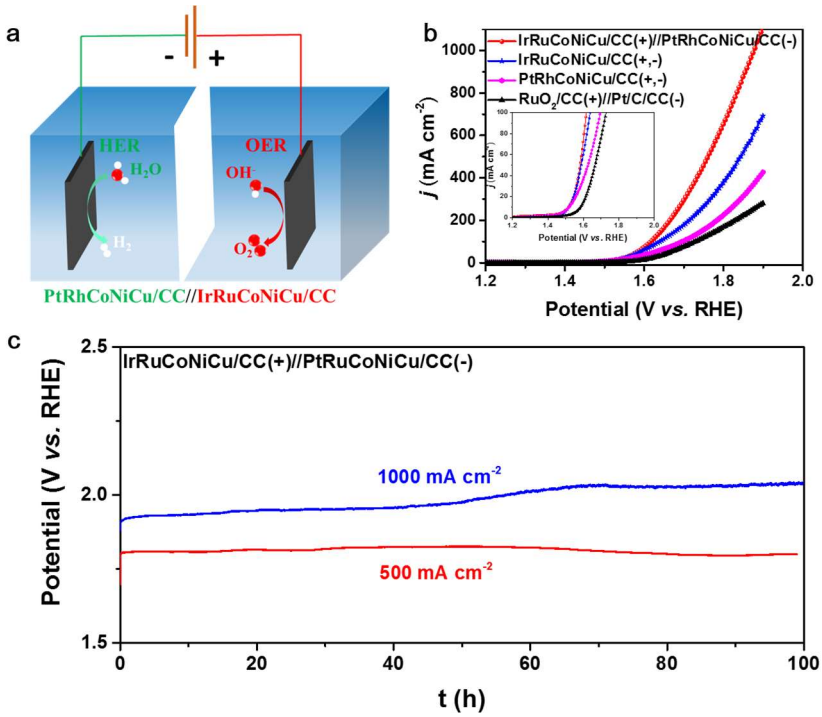

Figure 5. (a) Using IrRuCoNiCu/CC(+)//PtRhCoNiCu/CC(-) as the anode and cathode for water electrolysis. (b) LSV curves of water splitting for the investigated samples. (c) CP curves of IrRuCoNiCu/CC(+)//PtRhCoNiCu/CC(-) at 500 and 1000 mA cm^{-2}.

may be attributed to that Ir is the main active site, and the electronegativity of Fe, Co and Ni is lower than that of Ir and Ru, leading to redistribution of electron density and enhancement of Ir activity, while promoting the conversion of *OOH and the generation of O_2.[70] The excellent performance of IrRuCoNiCu/CC catalyst makes HEAs materials have broad application prospect in OER field.

The stability of IrRuCoNiCu/CC catalyst was studied by CP test. As shown in Figure 4f, the IrRuCoNiCu/CC catalyst exhibits excellent stability when tested at 1000 mA cm^{-2} for 150 h. In addition, comparing the LSV curves before and after 10,000 cycles (Figure S23), a negligible change is found. After stability testing, IrRuCoNiCu/CC catalyst remained its original morphology (Figure S24), indicating excellent stability. From XPS spectrum (Figure S25-S26), the catalyst surface was slightly oxidized during OER process. This may be due to the interaction between CC and NPs, which protects the active sites from over-oxidation during OER process, thereby improving the stability and activity of the catalyst.

For OER, we also prepared the Ru/CC and IrRu/CC (Figure S27). From Figure S28a and c, the OER activity of IrRuCoNiCu/CC catalyst was significantly higher than that of Ru/CC and IrRu/CC. Compared with Ru/CC (92.3 mV dev^{-1}) and IrRu/CC (78.2 mV dev^{-1}), Tafel slope value of IrRuCoNiCu/CC is smaller (69.1 mV dev^{-1}, Figure S28b), indicating the fast reaction dynamics of IrRuCoNiCu/CC. In addition, the Cdl of IrRuCoNiCu/CC, 32.0 mF cm^{-2}, is larger than that of Ru/CC (19.8 mF cm^{-2}) and IrRu/CC (23.9 mF cm^{-2}) (Figure S28d-f), indicating more active sites for IrRuCoNiCu/CC. The IrRuCoNiCu/CC shows a smaller semicircle diameter than Ru/CC and IrRu/CC (Figure S29), suggesting a faster electron transportation capacity.

Carbon-based materials have limited stability against oxidation at very oxidative potentials as those needed for OER.[71,72] To investigate the effect of these alloy NPs embedded in CC on catalytic activity and durability, alloy NPs were removed by acid leaching. OER activity decreased significantly due to the removal of alloy NPs during acid treatment (Figure S30). These results indicate that these alloy NPs have a certain contribution to OER. Metal alloy in alkaline medium is beneficial to improve the stability of catalyst. It is suggested that the intrinsic OER activity and stability of metal alloys may reduce the corrosion of carbon during OER by reducing the anodic polarization directly acting on the carbon itself.[71]

Based on the excellent performance of PtRhCoNiCu/CC (HER) and IrRuCoNiCu/CC (OER), a two-electrode system was used to evaluate the performance of water splitting (Figure 5a). As shown in Figure 5b, water splitting performance of IrRuCoNiCu/CC//PtRhCoNiCu/CC is superior to that of IrRuCoNiCu/CC, PtRhCoNiCu/CC and RuO_2/CC//Pt/C/CC. IrRuCoNiCu/CC//PtRhCoNiCu/CC shows excellent water splitting performance, reaching 1000 mA cm^{-2} at a low potential of 1.88 V. In addition, at 100 mA cm^{-2}, the potential of the IrRuCoNiCu/CC//PtRhCoNiCu/CC couple (1.61 V) is lower than the values for IrRuCoNiCu/CC couple (1.64 V), PtRhCoNiCu/CC couple (1.69 V) and RuO_2/CC//Pt/ C/CC couple (1.73 V). Impressively, the overall water splitting activity of the IrRuCoNiCu/CC//PtRhCoNiCu/CC electrolyzer is higher than that of most recently reported electrocatalysts (Table S5). From Figure 5c, the IrRuCoNiCu/CC//PtRhCoNiCu/CC can operate stably with slight fluctuations at 500 mA cm^{-2} high current densities for 100 h. However, a deactivation is observed from 50 h at

DOI: 10.14102/j.cnki.0254-5861.2022-0125

1000 mA cm^{-2}, which may be the formation of a large number of bubbles that cannot be removed in time during the reaction process, and the peeling of some of the catalytic active species from the carbon cloth substrate. These results indicate that the catalyst can be used as a candidate material for hydrogen production by industrial water splitting. In addition, the quantities of H_2 and O_2 are obtained at 0, 200, 400, 600, 800 and 1000 s by water drainage method at 50.0 mA. As shown in Figure S31, the volume ratio of H_2 and O_2 is about 2:1. With the increase of constant-current electrolysis time, H_2 (O_2) production changes linearly with time, and the amount of H_2 (O_2) production is close to the theoretical yield, indicating that the Faraday efficiency of water splitting is close to 100%.

CONCLUSION

In conclusion, we demonstrated the generation of a series of high entropy alloy nanoparticles embedded in carbon cloth by microwave heating. The generated HEA-NPs/CC were eventually used as electrocatalysts for HER, OER and water splitting, with significantly enhanced activity and stability due to the multiple active sites of HEA-NPs and the embedding of HEA-NPs into carbon support. Among them, PtRhCoNiCu/CC (HER:TOF = 0.49 s^{-1} at 100 mV overpotential, η_{10} = 19 mV and η_{1000} = 170 mV) and IrRuCoNiCu/CC (OER:TOF = 0.28 s^{-1} at 300 mV overpotential, η_{10} = 166 mV and η_{1000} = 354 mV) showed extraordinary HER and OER activities. And the two electrodes prepared by the catalyst were tested for water splitting. IrRuCoNiCu/CC(+)//PtRhCoNiCu/CC(-) can reach 1000 mA cm^{-2} high current density at 1.88 V, and exhibit excellent long-term stability. Microwave heating method has great potential in rapid preparation of multicomponent materials and can be developed to achieve large-scale production. In terms of expanding the scale of material preparation in the future, continuous processes can be developed to handle more reasonable yields and improve reproducibility; In situ characterization and measurement techniques are still to be improved, and the corresponding reaction mechanism is systematically studied, so as to provide guidance for industrial synthesis of nanomaterials; In chemical reaction process, how to accurately measure the internal temperature of microwave heating materials is still a challenge. It is necessary to establish an accurate microwave heating mechanism, more detailed theoretical analysis should be carried out, including modeling and simulation of microwave heating characteristics. In the future, microwave heating technology will meet the needs of high throughput synthesis in the fields of efficient energy storage and catalysis.

ACKNOWLEDGEMENTS

This work was supported by the National Natural Science Foundation of China (51772162, 22001143, and 52072197), Youth Innovation and Technology Foundation of Shandong Higher Education Institutions, China (2019KJC004), Outstanding Youth Foundation of Shandong Province, China (ZR2019JQ14), Taishan Scholar Young Talent Program (tsqn201909114, tsqn201909123), Natural Science Foundation of Shandong Province (ZR2020YQ34), Major Scientific and Technological Innovation Project (2019JZZY020405), and Major Basic Research Program of Natural Science Foundation of Shandong Province (ZR2020ZD09).

AUTHOR INFORMATION

Corresponding authors. Emails: inorchemwl@126.com (L. Wang) and jplai@qust.edu.cn (J. Lai)

COMPETING INTERESTS

The authors declare no competing interests.

ADDITIONAL INFORMATION

Supplementary information is available for this paper at http://manu30.magtech.com.cn/jghx/EN/10.14102/j.cnki.0254-5861.2022-0125

For submission: https://mc03.manuscriptcentral.com/cjsc

REFERENCES

(1) George, E. P.; Raabe, D.; Ritchie, R. O. High-entropy alloys. *Nat. Rev. Mater.* **2019**, 4, 515-534.

(2) Batchelor, T. A. A.; Pedersen, J. K.; Winther, S. H.; Castelli, I. E.; Jacobsen, K. W.; Rossmeisl, J. High-entropy alloys as a discovery platform for electrocatalysis. *Joule* **2019**, 3, 834-845.

(3) Lu, Z.; Chen, Z. W.; Singh, C. V. Neural network-assisted development of high-entropy alloy catalysts: decoupling ligand and coordination effects. *Matter* **2020**, 3, 1318-1333.

(4) Xin, Y.; Li, S.; Qian, Y.; Zhu, W.; Yuan, H.; Jiang, P.; Guo, R.; Wang, L. High-entropy alloys as a platform for catalysis: progress, challenges, and opportunities. *ACS Catal.* **2020**, 10, 11280-11306.

(5) Amiri, A.; Shahbazian-Yassar, R. Recent progress of high-entropy materials for energy storage and conversion. *J. Mater. Chem. A* **2021**, 9, 782-823.

(6) Li, H.; Lai, J.; Li, Z.; Wang, L. Multi-sites electrocatalysis in high-entropy alloys. *Adv. Funct. Mater.* **2021**, 31, 2106715.

(7) Sun, Y.; Dai, S. High-entropy materials for catalysis: a new frontier. *Sci. Adv.* **2021**, 7, eabg1600.

(8) Zhang, D.; Shi, Y.; Zhao, H.; Qi, W.; Chen, X.; Zhan, T.; Li, S.; Yang, B.; Sun, M.; Lai, J.; Huang, B.; Wang, L. Facile oil phase synthesis of multi-site synergistic high-entropy alloy to promote alkaline hydrogen evolution reaction. *J. Mater. Chem. A* **2021**, 9, 889-893.

(9) Li, T.; Dong, Q.; Huang, Z.; Wu, L.; Yao, Y.; Gao, J.; Wang, X.; Zhang, H.; Wang, D.; Li, T.; Shahbazian-Yassar, R.; Hu, L. Interface engineering between multi-elemental alloy nanoparticles and carbon support toward stable catalysts. *Adv. Mater.* **2022**, 32, 2106436.

(10) Masa, J.; Andronescu, C.; Schuhmann, W. Electrocatalysis as the nexus for sustainable renewable energy: the gordian knot of activity, stability, and selectivity. *Angew. Chem. Int. Ed.* **2020**, 59, 15298-15312.

(11) Huang, H.; Yan, M.; Yang, C.; He, H.; Jiang, Q.; Yang, L.; Lu, Z.; Sun, Z.; Xu, X.; Bando, Y.; Yamauchi, Y. Graphene nanoarchitectonics: recent advances in graphene-based electrocatalysts for hydrogen evolution reaction. *Adv. Mater.* **2019**, 31, 1903415.

(12) Karuppannan, M.; Kim, Y.; Gok, S.; Lee, E.; Hwang, J. Y.; Jang, J.-H.; Cho, Y.-H.; Lim, T.; Sung, Y.-E.; Kwon, O. J. A highly durable carbon-nanofiber-supported Pt-C core-shell cathode catalyst for ultra-low Pt loading proton exchange membrane fuel cells: facile carbon encapsulation. *Energy Environ. Sci.* **2019**, 12, 2820-2829.

(13) Zhang, J.; Zhang, Q.; Feng, X. Support and interface effects in

DOI: 10.14102/j.cnki.0254-5861.2022-0125

water-splitting electrocatalysts. *Adv. Mater.* **2019**, 31, 1808167.
(14) Gerber, I. C.; Serp, P. A theory/experience description of support effects in carbon-supported catalysts. *Chem. Rev.* **2020**, 120, 1250-1349.
(15) Li, C.-Z.; Wang, Z.-B.; Sui, X.-L.; Zhang, L.-M.; Gu, D.-M.; Gu, S. Graphitic carbon nitride nanosheet coated carbon black as a high-performance PtRu catalyst support material for methanol electrooxidation. *J. Mater. Chem. A* **2014**, 2, 20139-20146.
(16) Shao, Y.; Yin, G.; Gao, Y. Understanding and approaches for the durability issues of Pt-based catalysts for PEM fuel cell. *J. Power Sources* **2007**, 171, 558-566.
(17) Shi, W.; Zhang, B.; Lin, Y.; Wang, Q.; Zhang, Q.; Su, D. S. Enhanced chemoselective hydrogenation through tuning the interaction between Pt nanoparticles and carbon supports: insights from identical location transmission electron microscopy and X-ray photoelectron spectroscopy. *ACS Catal.* **2016**, 6, 7844-7854.
(18) Chen, Q.; Nie, Y.; Ming, M.; Fan, G.; Zhang, Y.; Hu, J.-S. Sustainable synthesis of supported metal nanocatalysts for electrochemical hydrogen evolution. *Chin. J. Catal.* **2020**, 41, 1791-1811.
(19) Van Deelen, T. W.; Hernández Mejía, C.; De Jong, K. P. Control of metal-support interactions in heterogeneous catalysts to enhance activity and selectivity. *Nat. Catal.* **2019**, 2, 955-970.
(20) Hu, S.; Li, W.-X. Sabatier principle of metal-support interaction for design of ultrastable metal nanocatalysts. *Science* **2021**, 374, 1360-1365.
(21) Sun, H.; Tung, C.-W.; Qiu, Y.; Zhang, W.; Wang, Q.; Li, Z.; Tang, J.; Chen, H.-C.; Wang, C.; Chen, H. M. Atomic metal-support interaction enables reconstruction-free dual-site electrocatalyst. *J. Am. Chem. Soc.* **2022**, 144, 1174-1186.
(22) Wu, X.; Wang, Z.; Zhang, D.; Qin, Y.; Wang, M.; Han, Y.; Zhan, T.; Yang, B.; Li, S.; Lai, J.; Wang, L. Solvent-free microwave synthesis of ultra-small Ru-Mo_2C@CNT with strong metal-support interaction for industrial hydrogen evolution. *Nat. Commun.* **2021**, 12, 4018.
(23) Shi, Y.; Ma, Z.-R.; Xiao, Y.-Y.; Yin, Y.-C.; Huang, W.-M.; Huang, Z.-C.; Zheng, Y.-Z.; Mu, F.-Y.; Huang, R.; Shi, G.-Y.; Sun, Y.-Y.; Xia, X.-H.; Chen, W. Electronic metal-support interaction modulates single-atom platinum catalysis for hydrogen evolution reaction. *Nat. Commun.* **2021**, 12, 3021.
(24) Li, Z.; Wu, R.; Zhao, L.; Li, P.; Wei, X.; Wang, J.; Chen, J. S.; Zhang, T. Metal-support interactions in designing noble metal-based catalysts for electrochemical CO_2 reduction: recent advances and future perspectives. *Nano Res.* **2021**, 14, 3795-3809.
(25) Zhang, J.; Ma, J.; Choksi, T. S.; Zhou, D.; Han, S.; Liao, Y.-F.; Yang, H. B.; Liu, D.; Zeng, Z.; Liu, W.; Sun, X.; Zhang, T.; Liu, B. Strong metal-support interaction boosts activity, selectivity, and stability in electrosynthesis of H_2O_2. *J. Am. Chem. Soc.* **2022**, 144, 2255-2263.
(26) Jayabal, S.; Saranya, G.; Geng, D.; Lin, L.-Y.; Meng, X. Insight into the correlation of Pt-support interactions with electrocatalytic activity and durability in fuel cells. *J. Mater. Chem. A* **2020**, 8, 9420-9446.
(27) Shilin, Z.; Liang, S.; Qining, F.; Fangli, Z.; Zhijie, W.; Jinshuo, Z.; Shiyong, Z.; Jianfeng, M.; Zaiping, G. Challenges and prospects of lithium-CO_2 batteries. *Nano Res. Energy* **2022**, https://doi.org/10.26599/NRE.2022.9120001.
(28) Kumar, R.; Sahoo, S.; Joanni, E.; Singh, R. K.; Kar, K. K. Microwave as a tool for synthesis of carbon-based electrodes for energy storage. *ACS Appl. Mater. Interfaces* **2021**, 14, 20306-20325.
(29) Lin, G.; Ju, Q.; Jin, Y.; Qi, X.; Liu, W.; Huang, F.; Wang, J. Suppressing dissolution of Pt-based electrocatalysts through the electronic metal-support interaction. *Adv. Energy Mater.* **2021**, 11, 2101050.
(30) Qiao, H.; Saray, M. T.; Wang, X.; Xu, S.; Chen, G.; Huang, Z.; Chen, C.; Zhong, G.; Dong, Q.; Hong, M.; Xie, H.; Shahbazian-Yassar, R.; Hu, L. Scalable synthesis of high entropy alloy nanoparticles by microwave heating. *ACS Nano* **2021**, 15, 14928-14937.
(31) Schwenke, A. M.; Hoeppener, S.; Schubert, U. S. Synthesis and modification of carbon nanomaterials utilizing microwave heating. *Adv. Mater.* **2015**, 27, 4113-4141.
(32) Yu, W.; Huang, H.; Qin, Y.; Zhang, D.; Zhang, Y.; Liu, K.; Zhang, Y.; Lai, J.; Wang, L. The synergistic effect of pyrrolic-N and pyridinic-N with Pt under strong metal-support interaction to achieve high-performance alkaline hydrogen evolution. *Adv. Energy Mater.* **2022**, 2200110.
(33) Zhao, H.; Zhang, D.; Yuan, Y.; Wu, X.; Li, S.; Li, Z.; Lai, J.; Wang, L. Rapid and large-scale synthesis of ultra-small immiscible alloy supported catalysts. *Appl. Catal. B Environ.* **2022**, 304, 120916.
(34) Xiong, G.; Jia, J.; Zhao, L.; Liu, X.; Zhang, X.; Liu, H.; Zhou, W. Non-thermal radiation heating synthesis of nanomaterials. *Sci. Bull.* **2021**, 66, 386-406.
(35) Ye, S.; Luo, F.; Zhang, Q.; Zhang, P.; Xu, T.; Wang, Q.; He, D.; Guo, L.; Zhang, Y.; He, C.; Ouyang, X.; Gu, M.; Liu, J.; Sun, X. Highly stable single Pt atomic sites anchored on aniline-stacked graphene for hydrogen evolution reaction. *Energy Environ. Sci.* **2019**, 12, 1000-1007.
(36) Bae, S.-Y.; Mahmood, J.; Jeon, I.-Y.; Baek, J.-B. Recent advances in ruthenium-based electrocatalysts for the hydrogen evolution reaction. *Nanoscale Horiz.* **2020**, 5, 43-56.
(37) Mu, X.; Gu, J.; Feng, F.; Xiao, Z.; Chen, C.; Liu, S.; Mu, S. RuRh bimetallene nanoring as high-efficiency pH-universal catalyst for hydrogen evolution reaction. *Adv. Sci.* **2021**, 8, 2002341.
(38) Wang, Q.; Ming, M.; Niu, S.; Zhang, Y.; Fan, G.; Hu, J.-S. Scalable solid-state synthesis of highly dispersed uncapped metal (Rh, Ru, Ir) nanoparticles for efficient hydrogen evolution. *Adv. Energy Mater.* **2018**, 8, 1801698.
(39) Wang, X.; Zheng, Y.; Sheng, W.; Xu, Z. J.; Jaroniec, M.; Qiao, S.-Z. Strategies for design of electrocatalysts for hydrogen evolution under alkaline conditions. *Mater. Today* **2020**, 36, 125-138.
(40) Hao, R.; Feng, Q.-L.; Wang, X.-J.; Zhang, Y.-C.; Li, K.-S. Morphology-controlled growth of large-area $PtSe_2$ films for enhanced hydrogen evolution reaction. *Rare Met.* **2022**, 41, 1314-1322.
(41) Peng, X.; Mi, Y.; Liu, X.; Sun, J.; Qiu, Y.; Zhang, S.; Ke, X.; Wang, X.; Luo, J. Self-driven dual hydrogen production system based on a bifunctional single-atomic Rh catalyst. *J. Mater. Chem. A* **2022**, 10, 6134-6145.
(42) Zhao, M.; Chen, Z.; Lyu, Z.; Hood, Z. D.; Xie, M.; Vara, M.; Chi, M.; Xia, Y. Ru octahedral nanocrystals with a face-centered cubic structure, {111} facets, thermal stability up to 400 °C, and enhanced catalytic activity. *J. Am. Chem. Soc.* **2019**, 141, 7028-7036.
(43) Cai, C.; Wang, M.; Han, S.; Wang, Q.; Zhang, Q.; Zhu, Y.; Yang, X.; Wu, D.; Zu, X.; Sterbinsky, G. E.; Feng, Z.; Gu, M. Ultrahigh oxygen evolution reaction activity achieved using Ir single atoms on amorphous CoO_x nanosheets. *ACS Catal.* **2021**, 11, 123-130.
(44) Shan, J.; Ling, T.; Davey, K.; Zheng, Y.; Qiao, S.-Z. Transition-metal-doped RuIr bifunctional nanocrystals for overall water splitting in acidic environments. *Adv. Mater.* **2019**, 31, 1900510.
(45) Shan, J.; Ye, C.; Chen, S.; Sun, T.; Jiao, Y.; Liu, L.; Zhu, C.; Song, L.; Han, Y.; Jaroniec, M.; Zhu, Y.; Zheng, Y.; Qiao, S.-Z. Short-range ordered iridium single atoms integrated into cobalt oxide spinel structure for highly efficient electrocatalytic water oxidation. *J. Am. Chem. Soc.* **2021**, 143, 5201-5211.

DOI: 10.14102/j.cnki.0254-5861.2022-0125

(46) Lyu, F.; Wang, Q.; Choi, S. M.; Yin, Y. Noble-metal-free electrocatalysts for oxygen evolution. *Small* **2019**, 15, 1804201.
(47) Anantharaj, S.; Aravindan, V. Developments and perspectives in 3d transition-metal-based electrocatalysts for neutral and near-neutral water electrolysis. *Adv. Energy Mater.* **2019**, 10, 1902666.
(48) Han, L.; Guo, L.; Dong, C.; Zhang, C.; Gao, H.; Niu, J.; Peng, Z.; Zhang, Z. Ternary mesoporous cobalt-iron-nickel oxide efficiently catalyzing oxygen/hydrogen evolution reactions and overall water splitting. *Nano Res.* **2019**, 12, 2281-2287.
(49) You, B.; Qiao, S. Z. Destabilizing alkaline water with 3d-metal (oxy)(hydr)oxides for improved hydrogen evolution. *Chem. Eur. J.* **2021**, 27, 553-564.
(50) Long, X.; Meng, J.; Gu, J.; Ling, L.; Li, Q.; Liu, N.; Wang, K.; Li, Z. Interfacial engineering of NiFeP/NiFe-LDH heterojunction for efficient overall water splitting. *Chin. J. Struct. Chem.* **2022**, 41, 2204046-2204053.
(51) Li, P.; Hong, W.; Liu W. Fabrication of large scale self-supported WC/Ni$(OH)_2$ electrode for high-current-density hydrogen evolution. *Chin. J. Struct. Chem.* **2021**, 40, 1365-1371.
(52) Wu, H, S.; Miao, T. F.; Shi, H. X.; Xu, Y.; Fu, X. L.; Qian, L. Probing photocatalytic hydrogen evolution of cobalt complexes: experimental and theoretical methods. *Chin. J. Struct. Chem.* **2021**, 40, 1696-1709.
(53) Yang, M.; Liu, Y.; Sun, J.; Zhang, S.; Liu, X.; Luo, J. Integration of partially phosphatized bimetal centers into trifunctional catalyst for high-performance hydrogen production and flexible Zn-air battery. *Sci. China Mater.* **2022**, 65, 1176-1186.
(54) Jin, Z.; Lv, J.; Jia, H.; Liu, W.; Li, H.; Chen, Z.; Lin, X.; Xie, G.; Liu, X.; Sun, S.; Qiu, H.-J. Nanoporous Al-Ni-Co-Ir-Mo high-entropy alloy for record-high water splitting activity in acidic environments. *Small* **2019**, 15, 1904180.
(55) Ma, P.; Zhang, S.; Zhang, M.; Gu, J.; Zhang, L.; Sun, Y.; Ji, W.; Fu, Z. Hydroxylated high-entropy alloy as highly efficient catalyst for electrochemical oxygen evolution reaction. *Sci. China Mater.* **2020**, 63, 2613-2619.
(56) Hua, W.; Sun, H.-H.; Xu, F.; Wang, J.-G. A review and perspective on molybdenum-based electrocatalysts for hydrogen evolution reaction. *Rare Met.* **2020**, 39, 335-351.
(57) Tauster, S. J.; Fung, S. C.; Garten, R. L. Strong metal-support interactions. Group 8 noble metals supported on titanium dioxide. *J. Am. Chem. Soc.* **1978**, 100, 170-175.
(58) Chen, K.; Wang, Z.; Wang, L.; Wu, X.; Hu, B.; Liu, Z.; Wu, M. Boron nanosheet-supported Rh catalysts for hydrogen evolution: a new territory for the strong metal-support interaction effect. *Nano-Micro. Lett.* **2021**, 13, 138.
(59) Zhang, W.; Yang, Y.; Huang, B.; Lv, F.; Wang, K.; Li, N.; Luo, M.; Chao, Y.; Li, Y.; Sun, Y.; Xu, Z.; Qin, Y.; Yang, W.; Zhou, J.; Du, Y.; Su, D.; Guo, S. Ultrathin PtNiM (M = Rh, Os, and Ir) nanowires as efficient fuel oxidation electrocatalytic materials. *Adv. Mater.* **2019**, 31, 1805833.
(60) Zhu, J.; Hu, L.; Zhao, P.; Lee, L. Y. S.; Wong, K.-Y. Recent advances in electrocatalytic hydrogen evolution using nanoparticles. *Chem. Rev.* **2020**, 120, 851-918.
(61) Yuan, L.-P.; Jiang, W.-J.; Liu, X.-L.; He, Y.-H.; He, C.; Tang, T.; Zhang, J.; Hu, J.-S. Molecularly engineered strong metal oxide-support interaction enables highly efficient and stable CO_2 electroreduction. *ACS Catal.* **2020**, 10, 13227-13235.
(62) Ritz, B.; Heller, H.; Myalitsin, A.; Kornowski, A.; Martin-Martinez, F. J.; Melchor, S.; Dobado, J. A.; Juárez, B. H.; Weller, H.; Klinke, C. Reversible attachment of platinum alloy nanoparticles to nonfunctionalized carbon nanotubes. *ACS Nano* **2010**, 4, 2438-2444.
(63) Rao, R. G.; Blume, R.; Hansen, T. W.; Fuentes, E.; Dreyer, K.; Moldovan, S.; Ersen, O.; Hibbitts, D. D.; Chabal, Y. J.; Schlögl, R.; Tessonnier, J.-P. Interfacial charge distributions in carbon-supported palladium catalysts. *Nat. Commun.* **2017**, 8, 340.
(64) Li, H.; Han, Y.; Zhao, H.; Qi, W.; Zhang, D.; Yu, Y.; Cai, W.; Li, S.; Lai, J.; Huang, B.; Wang, L. Fast site-to-site electron transfer of high-entropy alloy nanocatalyst driving redox electrocatalysis. *Nat. Commun.* **2020**, 11, 5437.
(65) Pan, C.-J.; Tsai, M.-C.; Su, W.-N.; Rick, J.; Akalework, N. G.; Agegnehu, A. K.; Cheng, S.-Y.; Hwang, B.-J. Tuning/exploiting strong metal-support Interaction (SMSI) in heterogeneous catalysis. *J. Taiwan Inst. Chem. E* **2017**, 74, 154-186.
(66) Löffler, T.; Savan, A.; Garzón-Manjón, A.; Meischein, M.; Scheu, C.; Ludwig, A.; Schuhmann, W. Toward a paradigm shift in electrocatalysis using complex solid solution nanoparticles. *ACS Energy Lett.* **2019**, 4, 1206-1214.
(67) Löffler, T.; Savan, A.; Meyer, H.; Meischein, M.; Strotkötter, V.; Ludwig, A.; Schuhmann, W. Design of complex solid-solution electrocatalysts by correlating configuration, adsorption energy distribution patterns, and activity curves. *Angew. Chem. Int. Ed.* **2020**, 59, 5844-5850.
(68) Shi, W.; Liu, H.; Li, Z.; Li, C.; Zhou, J.; Yuan, Y.; Jiang, F.; Fu, K.; Yao, Y. High-entropy alloy stabilized and activated Pt clusters for highly efficient electrocatalysis. *SusMat* **2022**, 2, 186-196.
(69) Li, H.; Sun, M.; Pan, Y.; Xiong, J.; Du, H.; Yu, Y.; Feng, S.; Li, Z.; Lai, J.; Huang, B.; Wang, L. The self-complementary effect through strong orbital coupling in ultrathin high-entropy alloy nanowires boosting pH-universal multifunctional electrocatalysis. *Appl. Catal. B Environ.* **2022**, 312, 121431.
(70) Zhu, H.; Zhu, Z.; Hao, J.; Sun, S.; Lu, S.; Wang, C.; Ma, P.; Dong, W.; Du, M. High-entropy alloy stabilized active Ir for highly efficient acidic oxygen evolution. *Chem. Eng. J.* **2021**, 431, 133251.
(71) Gupta, S.; Qiao, L.; Zhao, S.; Xu, H.; Lin, Y.; Devaguptapu, S. V.; Wang, X.; Swihart, M. T.; Wu, G. Highly active and stable graphene tubes decorated with FeCoNi alloy nanoparticles via a template-free graphitization for bifunctional oxygen reduction and evolution. *Adv. Energy Mater.* **2016**, 6, 1601198.
(72) Zheng, X.; Cao, X.; Sun, Z.; Zeng, K.; Yan, J.; Strasser, P.; Chen, X.; Sun, S.; Yang, R. Indiscrete metal/metal-N-C synergic active sites for efficient and durable oxygen electrocatalysis toward advanced Zn-air batteries. *Appl. Catal. B Environ.* **2020**, 272, 118967.

Received: May 16, 2022
Accepted: May 26, 2022
Published online: June 2, 2022
Published: July 25, 2022

DOI: 10.14102/j.cnki.0254-5861.2022-0125